Contribution from Lash Miller Chemistry Laboratories and Erindale College, University of Toronto, Toronto, Ontario, Canada

Direct Synthesis Using Vanadium Atoms. 3. Binary Carbonyls of Vanadium, $V(CO)_n$ (where n = 1–5)

L. HANLAN, H. HUBER, and G. A. OZIN*

Received February 18, 1976 AIC60128Z

The series of d^5 binary vanadium carbonyls $V(CO)_n$ (where n = 1–5) has been synthesized in various low-temperature matrices using V atom–CO cocondensation reactions. Matrix infrared spectroscopy in combination with V and CO concentration studies, annealing experiments, $^{12}C^{16}O/^{13}C^{16}O$ isotopic substitution, and frequency calculations serves to identify the mononuclear complexes. The observed geometries for n = 3, 4, and 5 are discussed in the light of recent theoretical predictions. Extended Hückel molecular orbital calculations are reported for V(CO) and $V(CO)_2$ as a function of the ∠VCO and ∠CVC angles in the range 90 to 180° in an effort to rationalize the anomalously high ν(CO) stretching frequency of V(CO) and the remarkable observation of three mononuclear $V(CO)_2$ complexes in Ar, Kr, and Xe matrices.

Introduction

It has recently been reported that $V(CO)_6$ can be directly synthesized from V atoms and CO at 10 K.[1] At vanadium concentrations exceeding 1 atom %, spectroscopic evidence was obtained for the elusive dimer $V_2(CO)_{12}$.[1] The formation of the dimer under these conditions was not unexpected in view of the pronounced tendency of V atoms to diffuse and dimerize on deposition with Ar at 10 K.[2]

In this paper we present infrared spectroscopic data for the d^5 binary carbonyl intermediates, $V(CO)_n$ (where n = 1–5), which are formed when V atoms are cocondensed with CO diluted in noble gas matrices at 6–10 K.

Experimental Section

Monatomic V was generated by directly heating a thin vanadium filament (0.025 in.). The vanadium metal (99.99%) was supplied by A. D. McKay, New York, N.Y. Research grade $^{12}C^{16}O$, Ne, Ar, Kr, and Xe (99.99%) were supplied by Matheson of Canada and $^{12}C^{16}O/^{13}C^{16}O$ isotopic mixtures by Stohler, Montreal, Canada. The furnace used for the evaporation of the metals has been described previously.[3] The rate of metal atom deposition was continuously monitored using a quartz crystal microbalance.[4] To obtain quantitative data for V/CO/M (M = Ne, Ar, Kr, Xe) cocondensations, it was necessary to calibrate carefully the rate of deposition of both metal and gas onto the sample window as described previously.[5] For the infrared experiments, matrices were deposited on a CsI plate cooled to 10–12 K by means of an Air Products Displex closed-cycle helium refrigerator or to 6 K by a liquid helium transfer system. Infrared spectra were recorded on a Perkin-Elmer 180 or 621 spectrophotometer. Our molecular orbital calculations for VCO and $V(CO)_2$ were of the extended Hückel type [6] with charge iteration. We used the 3d, 4s, and 4p orbitals of atomic V and the 2s and 2p orbitals of C and O, Clementi–Raimondi [7] and Richardson et al. [8] orbital exponents, the Cusachs' approximation [9] and known values for the Coulomb integrals.[10] The parameters required to reproduce our extended Hückel calculations are tabulated in Chart I.

Chart I

	Orbital	Orbital exponent[a]	H_{ii}, eV[a]
V	3d	2.994	−8.85
	4s	1.245	−7.49
	4p	1.150	−4.46
C	2s	1.608	−19.42
	2p	1.568	−10.64
O	2s	2.246	−32.33
	2p	2.227	−15.80

r(V-C) = 1.890 Å; r(C-O) = 1.128 Å

[a] The calculations were performed using an IBM 370 computer.

Experimental Results

On cocondensing V atoms with CO/Ar ≃ 1/10 mixtures at 8–10 K under conditions of low metal concentration, the infrared spectrum shown in Figure 1 was obtained. Besides the known $V(CO)_6$ doublet at 1976/1970 cm^{-1},[1] *four* new CO stretching modes were observed at 1952, 1943, 1920, and 1893 cm^{-1} (the absence of weak absorptions at frequencies above those of $V(CO)_6$ is noteworthy). The doublet at 1952/1943 cm^{-1} appeared with the same intensity ratio (ca. 2:3) on deposition and during 10–40 K annealing experiments. On the other hand, the two ν(CO) stretching modes at 1920 and 1893 cm^{-1} had a different intensity behavior with respect to each other and the aforementioned 1952/1943-cm^{-1} doublet. During warm-up of CO/Ar ≃ 1/10 matrices, the absorption at 1920 cm^{-1} decreased in intensity, followed by the 1893-cm^{-1} line and then the 1952/1943-cm^{-1} doublet. At 35–40 K $V(CO)_6$ was the major absorbing species with trace amounts of the dimer $V_2(CO)_{12}$ as seen by the growth of weak ν(CO) absorptions at 2048, 2028, and 2014 cm^{-1}.[1] When the CO/Ar ≃ 1/10 deposition was conducted at 15–20 K the major difference from the previous runs was the formation of some $V_2(CO)_{12}$ in addition to $V(CO)_6$ and the species absorbing at 1952/1943 (V), 1920 (III), and 1893 (IV).

When the less rigid matrix support CO/Ne ≃ 1/10 was used at 6–8 K, the results were similar to those obtained in CO/Ar ≃ 1/10 at 15–20 K, except that species V and IV appeared with lower intensities relative to $V(CO)_6$, and species III was absent.

These results imply that besides $V(CO)_6$ three other mononuclear vanadium carbonyls can be formed by depositing V atoms into concentrated CO/Ar matrices. On warming the matrices to 35–40 K, $V(CO)_n$ are gradually converted to $V(CO)_6$ together with a small amount of $V_2(CO)_{12}$. Diffusion and dimerization to $V_2(CO)_{12}$ can be induced either by raising the deposition temperature to 15–20 K in CO/Ar ≃ 1/10 matrices or by working in the more mobile matrix CO/Ne ≃ 1/10 at 6–8 K.

A reasonable a priori assignment of the new species is therefore: V ≡ $V(CO)_5$, IV ≡ $V(CO)_4$, III ≡ $V(CO)_3$.

To obtain support for these assignments and evidence for species having n = 1 and 2, the experiments were repeated in CO/Ar ≃ 1/50 matrices at 8–10 K. A typical infrared spectrum obtained at low concentrations of metal (V/Ar ≃ 10^{-4}) is shown in Figure 2A and can be seen to be quite different from those obtained in CO/Ar ≃ 1/10 matrices under comparable deposition conditions (Figure 1).

A vanadium concentration study was performed in CO/Ar ≃ 1/50 matrices with V/Ar in the range $1/10^5$ to $1/10^2$ (see, for example, Figure 2B) and showed that absorptions at 2021/2014/2011, 1873, 1825, and 1810/1802 cm^{-1} are associated with binuclear or higher clusters, $V_x(CO)_y$, while those at 1974, 1904, 1882, 1820, and 1723/1719 cm^{-1} are associated with mononuclear species, $V(CO)_n$, where $n < 3$ (Figure 2A). When CO/Ar ≃ 1/50 matrices which were essentially free of $V_x(CO)_y$ species were annealed in the range 10–40 K, the absorptions attributed to $V(CO)_6$ (1976/1970

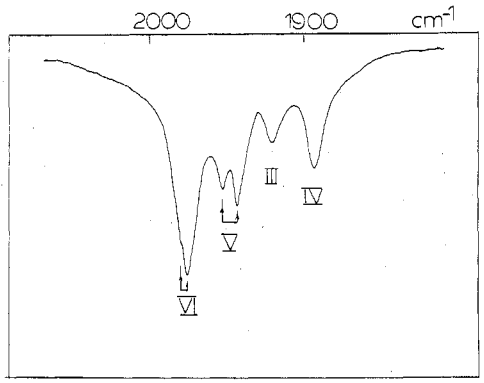

Figure 1. The matrix infrared spectrum of the products formed on cocondensing V atoms with CO/Ar ≃ 1/10 matrices at 8–10 K under conditions of low metal concentration (V/Ar ≃ $1/10^4$) showing $V(CO)_6$ (VI), $V(CO)_5$ (V), $V(CO)_4$ (IV), and $V(CO)_3$ (III).

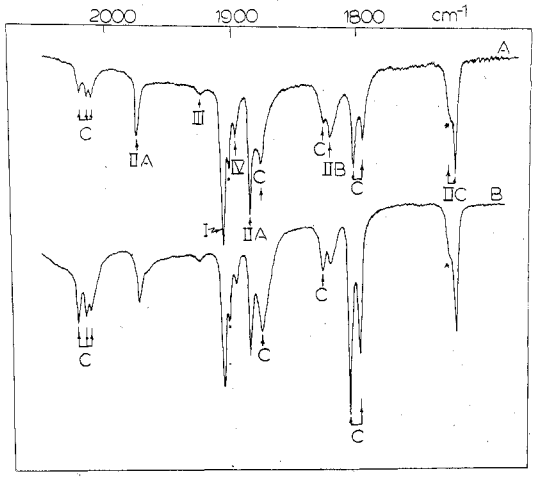

Figure 2. The matrix infrared spectrum of the products formed on cocondesing V atoms with CO/Ar ≃ 1/50 mixtures at 8–10 K: (A) under conditions of low metal concentration (V/Ar ≃ $1/10^4$) showing $V(CO)_2$ (IIA, IIB, and IIC) and V(CO) (I); and (B) under conditions of higher metal concentration (V/Ar ≃ $2.7/10^4$) showing which absorptions can be associated with $V_x(CO)_y$ cluster species (C).

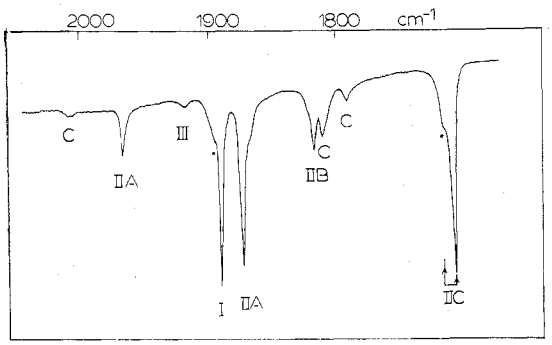

Figure 3. The matrix infrared spectrum of the products formed on cocondensing V atoms with CO/Kr ≃ 1/50 mixtures (V/Kr ≃ $1/10^4$) at 8–10 K (same notation as Figure 2). The weak shoulders marked with an asterisk were shown from isotopic substitution experiments to arise from multiple trapping site effects.

cm^{-1}), $V(CO)_5$ (1952/1943 cm^{-1}), $V(CO)_4$ (1893 cm^{-1}), and $V(CO)_3$ (1920 cm^{-1}) were observed to grow in, indicating that the new CO absorptions at 1974, 1904, 1882, 1820, and 1723/1719 cm^{-1} are linked to $V(CO)_2$ and V(CO) species.

To minimize diffusion and aggregation problems[11] and to simplify $^{12}C^{16}O/^{13}C^{16}O$ isotope substitution experiments, the more rigid matrices Kr and Xe were employed. For example, when V atoms were cocondensed with CO/Kr ≃ 1/50 mixtures at 10 K, the infrared spectrum showed three intense lines[25] at 1890, 1874, and 1707 cm^{-1} with two weaker lines at 1968 and 1816 cm^{-1} (Figure 3). Matrix annealing experiments in the range 10–65 K showed a number of interesting features which are summarized below: (a) The 1968- and 1874-cm^{-1} absorptions belong to a single species. (b) The 1890-cm^{-1} absorption is almost coincident with the 1885-cm^{-1} absorption of species IV, the latter making itself apparent at 40 K. (c) At 45 K absorptions grow in at 1974/1968 (VI), 1947/1939 (V), 1917 (III), and 1885 (IV), which can be identified with the corresponding species identified in Ar matrices.

Because the CO/Kr ≃ 1/50 infrared spectrum is reasonably simple, the corresponding $^{12}C^{16}O/^{13}C^{16}O/Kr$ ≃ 1/1/50 experiment was performed. The isotope patterns shown in Figure 4 are consistent with the assignments in Chart II. When the experiment was repeated using $^{12}C^{16}O/^{13}C^{16}O/Kr$ = 1/1/250 mixtures, the major absorbing species were

Chart II

(I)	1890 $V^{12}C^{16}O$	(IIB)	1816 $V(^{12}C^{16}O)_2$
	1848 $V^{13}C^{16}O$		1792 $V(^{12}C^{16}O)(^{13}C^{16}O)$
(IIA)	1968 $V(^{12}C^{16}O)_2$		1778 $V(^{13}C^{16}O)_2$
	1940 $V(^{12}C^{16}O)(^{13}C^{16}O)$	(IIC)	1707 $V(^{12}C^{16}O)_2$
	1919 $V(^{13}C^{16}O)_2$		1686 $V(^{12}C^{16}O)(^{13}C^{16}O)$
	1874 $V(^{12}C^{16}O)_2$		1674 $V(^{13}C^{16}O)_2$
	1854 $V(^{12}C^{16}O)(^{13}C^{16}O)$		
	1830 $V(^{13}C^{16}O)_2$		

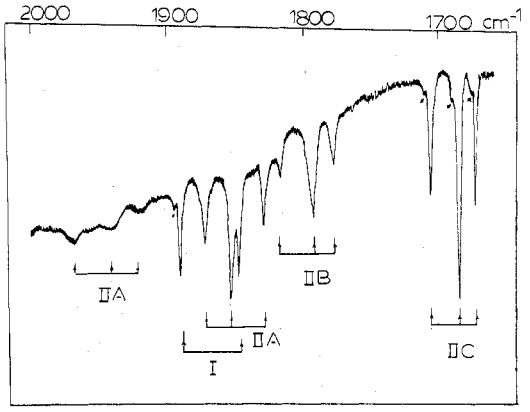

Figure 4. The matrix infrared spectrum of the products formed on cocondensing V atoms with $^{12}C^{16}O/^{13}C^{16}O/Kr$ ≃ 1/1/50 mixtures (V/Kr < $1/10^4$) at 8–10 K. The weak shoulders marked with an asterisk were shown from isotopic substitution experiments to arise from multiple trapping site effects.

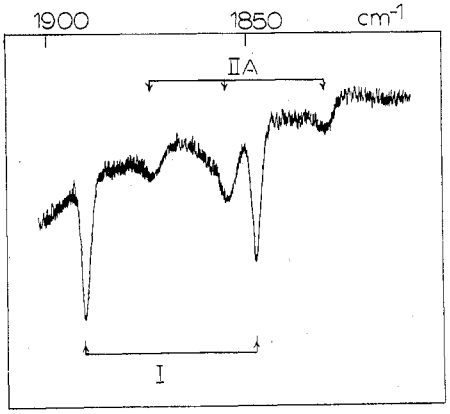

Figure 5. The same as Figure 4 except that $^{12}C^{16}O/^{13}C^{16}O/Kr$ ≃ 1/1/250 mixtures were employed.

Table I. Characteristic CO Stretching Modes of $V(CO)_n$ (where n = 1–5) in Ar, Kr, and Xe Matrices[a–c]

Matrix	$V(CO)_5$ (V)	$V(CO)_4$ (IV)	$V(CO)_3$ (III)	$V(CO)_2$ (IIA)[e]	$V(CO)_2$ (IIB)[e]	$V(CO)_2$ (IIC)[d,e]	V(CO) (I)
Ar	1952/1943	1893	1920	1974/1882	1820	1723/1719	1904
Kr	1947/1939	1885	1917	1968/1874	1816	1712/1707	1890
Xe	1944/1935	1881	1914	1960/1862	1814	1704/1699	1868

[a] Small concentration and temperature-dependent shifts of the order of ±2 cm^{-1} were observed on most absorptions in the M/A range 1/10 to 1/250. Average values are quoted in the above table. [b] Frequencies in cm^{-1}. [c] Absorptions associated with $V_x(CO)_y$ aggregate species were identified by vanadium concentration experiments at 2021, 2014, 2011, 1873, 1825, 1810, and 1802 cm^{-1}. [d] Shown to be a matrix splitting from $^{12}C^{16}O/^{13}C^{16}O$ isotopic substitution. [e] The frequency data for the three forms of $V(CO)_2$ in Ar, Kr, and Xe give linear Buckingham plots (see ref 20) which are more consistent with the idea of three different forms of $V(CO)_2$ (IIA, IIB, and IIC) rather than specific $V(CO)_2$... noble gas complexes.

Table II. Predicted and Observed Geometries for $V(CO)_n$ Species (where n = 1–6)

	$V(CO)_6$	$V(CO)_5$	$V(CO)_4$	$V(CO)_3$	$V(CO)_2$	V(CO)
Hoffmann's MO calculation[4]		C_{4v}[a]	C_{2v}[a]	C_{3v}[a]		
Burdett's MIE calculation[3]	O_h	D_{3h}[a]	C_{2v},[a] D_{4h},[b] T_d[c]	C_{3v},[a] C_{2v},[b] D_{3h}[c]	C_{2v}[a,b]	
Burdett's hole-pair overlap calculations[5]	O_h	C_{4v}[a]	C_{2v}[a]	C_{3v}[a]	C_{2v}[a]	
Jahn–Teller considerations	D_{4h} or D_{3d}	C_{2v}[a]	C_{2v}[a]	C_{3v},[a] C_{2v}[b]	C_{2v}[a]	C_s[a]
Obsd geometry	O_h[d]	D_{3h}[e]	T_d or D_{4h}	D_{3h} or C_{3v}	C_{2v} and $D_{\infty h}$	C_s

[a] Low spin. [b] Intermediate spin. [c] High spin. [d] Essentially octahedral as a result of a dynamic Jahn–Teller effect. [e] Synthesized by V/CO matrix cocondensation reactions (this study) and independently by $V(CO)_6$/Ar matrix photolysis.[7]

Chart III

(I)	1868	$V^{12}C^{16}O$	(IIB) 1814	$V(^{12}C^{16}O)_2$
	1825	$V^{13}C^{16}O$	1790	$V(^{12}C^{16}O)(^{13}C^{16}O)$
(IIA)	1960	$V(^{12}C^{16}O)_2$	1776	$V(^{13}C^{16}O)_2$
	1862	$V(^{12}C^{16}O)_2$	(IIC) 1698	$V(^{12}C^{16}O)_2$
	1843	$V(^{12}C^{16}O)(^{13}C^{16}O)$	1677	$V(^{12}C^{16}O)(^{13}C^{16}O)$
	1819	$V(^{13}C^{16}O)_2$	1661	$V(^{13}C^{16}O)_2$

Chart IV

Kr	Xe	Assignment
1917	1914	$V(^{12}C^{16}O)_3$
1900	1898	$V(^{12}C^{16}O)(^{13}C^{16}O)_2$
1886	1883	$V(^{12}C^{16}O)_2(^{13}C^{16}O)$
1873	1868	$V(^{13}C^{16}O)_3$

$V^{12}C^{16}O/V^{13}C^{16}O$ at 1890/1848 cm^{-1} (Figure 5).

An intriguing aspect of the CO/Kr experiments is the formation of *three* mononuclear dicarbonyls. Experiments performed in dilute CO/Xe matrices yielded similar results which led to the parallel assignments in Chart III.

Annealing experiments in CO/Xe ≃ 1/50 matrices in the range 10–75 K served to identify the higher carbonyl species at 1976/1966 (VI), 1944/1935 (V), 1881 (IV), and 1914 (III).

Owing to complex overlapping problems in all of the matrices studied, definitive isotope patterns could not be established for species V and IV. However, in dilute Kr and Xe matrices (after warm-up to 30–40 °K), isotope lines could be extracted for species III as shown in Chart IV.

Vanadium Carbonyl Aggregates

When vanadium atoms were cocondensed with CO/Ar ≃ 1/50 mixtures (V/Ar ≃ $1/10^5$ to $1/10^2$) at 6–10 K and the resulting infrared spectra recorded as a function of the $[V]_0$ concentration (as described earlier), the carbonyl stretching modes associated with the $V(CO)_n$ complexes (where n = 1–6) could be distinguished from those of $V_x(CO)_y$ cluster complexes on the basis of the absorbance ratios $I_{V_x(CO)_y}/I_{V(CO)_n}$.[2] Infrared lines assigned to vanadium carbonyl aggregates are listed in Table I. An interesting aspect of these experiments relates to the increasing complexity of the region centered around 2000 cm^{-1} with increasing concentration of vanadium in the matrix. A gradual transformation was observed from a series of narrow absorptions ($\Delta\nu_{1/2}$ ≃ 5 cm^{-1}) at 2021/2014/2011 cm^{-1} for V/Ar ≃ $1/10^4$ to a broad, structured absorption ($\Delta\nu_{1/2}$ ≃ 100 cm^{-1}) centered at about 1990 cm^{-1} for V/Ar ≃ $1/10^2$. These changes most probably reflect the smooth transition from a system containing CO coordinated to small vanadium clusters, $V_x(CO)_y$ (where x ≃ 2), to ones in which the CO is bonding to larger vanadium clusters ($x > 2$). This can be seen from the close resemblance of the high $[V]_0$ infrared spectra to those of CO chemisorbed on vanadium metallic films, the latter showing a very broad absorption centered at 1940 cm^{-1}.[12]

It would therefore appear that experiments of this type are capable of producing small, well-defined clusters and cluster complexes which should serve as useful models for studying the chemisorbed state.

Discussion of Results

Burdett[13] and Hoffmann[14] have reported theoretical models to rationalize the shapes of binary transition metal complexes. The calculations, upon which their geometric conclusions are based, are of the extended Hückel type with minimum energy criteria. Different structures are rationalized by reference to the energy changes of the relevant molecular orbitals which occur on adjusting the molecular geometry. The minimum internal energy (MIE) geometry is that structure at which the overall metal–ligand overlap for the occupied metal d orbitals is optimized. More recently, Burdett[15] has presented a related scheme based on overlap between ligand σ pairs and the holes in a nonspherically symmetrical charge distribution to rationalize geometries either predicted by MIE criteria or observed experimentally. The hole-pair theory[15] can be regarded as an extension of the well-known Gillespie–Nyholm VSEPR method[16] commonly employed to rationalize the geometries of main group compounds to include binary transition metal complexes.

With some exceptions, Burdett's orbital overlap and Jahn–Teller arguments,[13] Hoffmann's molecular orbital calculations,[14] as well as Burdett's hole-pair overlap theory[15] lead to the same general conclusions for the known binary carbonyl complexes, $M(CO)_n$ (Table II). The results of the present study for the new series of d^5 $V(CO)_n$ complexes are summarized in Table II together with their predicted geometries. A brief discussion of each complex follows.

Vanadium Pentacarbonyl, $V(CO)_5$. In practice, there seems to be general agreement that $V(CO)_5$, produced by either matrix photochemical or metal atom techniques,

$$V(CO)_6/Ar \xrightarrow[15\ K]{h\nu} V(CO)_5 \quad \text{(ref 17)}$$

$$V/CO/Ar \xrightarrow[10\ K]{} V(CO)_5 \quad \text{(this study)}$$

has trigonal bipyramidal (D_{3h}) symmetry.

On the basis of Jahn–Teller arguments, both the D_{3h} and C_{4v} configurations of $V(CO)_5$ are predicted to be unstable and an intermediate C_{2v} structure should be found. However, MIE and hole-pair calculations[13-15] indicate that the difference in energy between the D_{3h} and C_{4v} structures of $V(CO)_5$ is expected to be small. In this context we note that the Jahn–Teller effect in d^5 $V(CO)_6$ is small and gives rise experimentally to a dynamical effect and an essentially O_h molecule.[1,13,15,18] It is therefore not inconceivable that matrix solid state effects may be responsible for the observed structure, although the occurrence of the D_{3h} $V(CO)_5$ in Ar, Kr, and Xe matrices would argue in favor of the D_{3h} form being truly representative of the equilibrium configuration of the molecule.

Vanadium Tetracarbonyl, $V(CO)_4$. Vanadium tetracarbonyl as synthesized from V atom matrix reactions presents two experimental problems. First, it displays just a single observable $\nu(CO)$ stretching mode. Second, overlap problems prevent the obtaining of useful isotope data. Theoretically, there is general agreement that the low-spin molecule should have a C_{2v} structure with opposite angles of 160 and 100°.[13,14] The single absorption observed for $V(CO)_4$ can therefore be taken to imply that either some lines have been obscured through band overlap or simply missed because of their low intensities. If this is not the case then one will be forced to conclude that the molecule is of a higher symmetry than C_{2v}, and thus D_{4h} (intermediate spin) and T_d (high spin) geometries in Burdett's terminology[13] will become possible candidates. Clarification of this point will require additional experimental data.

Vanadium Tricarbonyl, $V(CO)_3$. The planarity of the $M(CO)_3$ species (or linearity of $M(CO)_2$ species) is usually determined by the nonobservation of the totally symmetrical CO stretching vibration in the infrared spectrum. This procedure, however, can be fraught with danger since, for near-planar $M(CO)_3$ (or near-linear $M(CO)_2$) structures, the symmetrical CO stretching vibration is expected to be extremely weak compared to its asymmetric counterpart vibration and may pass undetected in the infrared spectrum, even though isotopic data can help pinpoint the position of the symmetric mode. The observation of a single infrared-active CO stretching vibration which can be definitely associated with $V(CO)_3$ by virtue of its CO concentration dependence, matrix annealing behavior, and calculated and observed $^{12}C^{16}O/^{13}C^{16}O$ isotope pattern (see Table III) can be taken as evidence in favor of the D_{3h} trigonal planar geometry. However, in the light of the C_{3v} predictions for low-spin $V(CO)_3$,[13-15] definitive proof of this structure will also require additional experimental data.

Vanadium Dicarbonyl, $V(CO)_2$. The formation of vanadium dicarbonyl in dilute CO/Ar, CO/Kr, and CO/Xe matrices yields the intriguing experimental observation that the molecule can be trapped in *three* distinct forms, referred to earlier as IIA, IIB and IIC in order of decreasing CO stretching frequencies.

In order to check the validity of our dicarbonyl assignments, frequency calculations based on a Cotton–Kraihanzel force field[19] were performed on the $^{12}C^{16}O/^{13}C^{16}O$ mixed isotopic molecules of IIA, IIB, and IIC. The agreement between the observed and calculated frequencies for the three forms of the dicarbonyl (Table IV) is found to be satisfactory for all observed CO stretching modes and provides convincing support for our vibrational assignments.

Although Cotton–Kraihanzel-type calculations are expected to be insensitive to conformational changes in a dicarbonyl complex, it would appear that the high-frequency form IIA is best assigned to a noncentrosymmetric dicarbonyl on the grounds that both the symmetric and asymmetric CO stretching modes are infrared active (Table I). On the other hand, the intermediate-frequency IIB and low-frequency IIC forms show just a single CO stretching mode (Table I) and favor centrosymmetric forms of the molecule. An a priori formulation for the three forms of the dicarbonyl is the following:

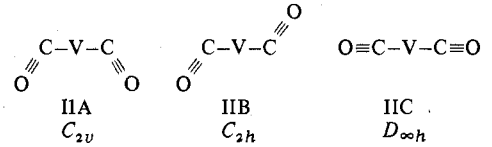

IIA (C_{2v}) IIB (C_{2h}) IIC ($D_{\infty h}$)

Table III. Observed and Calculated Frequencies[a] (cm^{-1}) for $V(^{12}C^{16}O)_n(^{13}C^{16}O)_{3-n}$ (where n = 0–3) in Kr and Xe Matrices

Krypton		Xenon		
Obsd	Calcd[b]	Obsd	Calcd[b]	Assignment
1917	1916.3	1914	1912.9	$V(^{12}C^{16}O)_3$ (E′) + $V(^{12}C^{16}O)_2(^{13}C^{16}O)$ (B_2)
1900	1899.9	1898	1896.3	$V(^{12}C^{16}O)(^{13}C^{16}O)_2$ (A_1)
1886	1886.0	1883	1882.5	$V(^{12}C^{16}O)_2(^{13}C^{16}O)$ (A_1)
1873	1873.7	1868	1870.4	$V(^{13}C^{16}O)_3$ + $V(^{12}C^{16}O)(^{13}C^{16}O)_2$ (B_2)

[a] Best fit C.K. force constants obtained from this analysis are k_{CO} = 15.86 and $k_{CO,CO}$ = 1.07 mdyn/Å in Kr and k_{CO} = 16.06 and $k_{CO,CO}$ = 1.22 mdyn/Å in Xe matrices. [b] High-frequency, in-phase, infrared-active CO stretching modes were calculated at 2125.7 and 2110.2 cm^{-1} in Kr and 2097.5 and 2082.2 cm^{-1} in Xe matrices and were probably not observed because of band overlap problems in the 2150–2000-cm^{-1} region.

Table IV. Observed and Calculated Frequencies for $V(^{12}C^{16}O)_n(^{13}C^{16}O)_{2-n}$ (where n = 0–2) in Krypton and Xenon Matrices

Krypton		Xenon		Assignment[b] (C_{2v} structure)
Obsd	Calcd	Obsd	Calcd	
		Molecule IIa		
1968	1962.7	1960	1960.3	$V(^{12}C^{16}O)_2$ (A_1)
1940	1945.8	*a*	1943.0	$V(^{12}C^{16}O)(^{13}C^{16}O)$ (A′)
1919	1919.1	*a*	1916.7	$V(^{13}C^{16}O)_2$ (A_1)
1874	1875.0	1862	1863.4	$V(^{12}C^{16}O)_2$ (B_2)
1854	1849.2	1843	1841.2	$V(^{12}C^{16}O)(^{13}C^{16}O)$ (A″)
1830	1833.3	1819	1922.0	$V(^{13}C^{16}O)_2$ (B_2)
k_{CO} = 14.88		k_{CO} = 14.77		
k_{COCO} = 0.68		k_{COCO} = 0.75		
		Molecule IIB		
				(C_{2h} structure)[b]
c	1898.4	*c*	1896.8	$V(^{12}C^{16}O)_2$ (A_g)
a	1882.3	*a*	1880.7	$V(^{12}C^{16}O)(^{13}C^{16}O)$ (A′)
c	1856.3	*c*	1854.1	$V(^{13}C^{16}O)_2$ (A_g)
1816	1817.2	1814	1815.1	$V(^{12}C^{16}O)_2$ (B_u)
1792	1792.0	1790	1790.0	$V(^{12}C^{16}O)(^{13}C^{16}O)$ (A″)
1778	1776.8	1776	1774.8	$V(^{13}C^{16}O)_2$ (B_u)
k_{CO} = 13.95		k_{CO} = 13.92		
k_{COCO} = 0.61		k_{COCO} = 0.61		
		Molecule IIC		
				($D_{\infty h}$ structure)[b]
c	1791.2	*c*	1799.8	$V(^{12}C^{16}O)_2$ (Σ_g^+)
a	1775.7	*a*	1781.6	$V(^{12}C^{16}O)(^{13}C^{16}O)$ (Σ^+)
c	1751.4	*c*	1757.9	$V(^{13}C^{16}O)_2$ (Σ_g^+)
1707	1709.4	1698	1698.8	$V(^{12}C^{16}O)_2$ (Σ_u^+)
1686	1686.0	1677	1676.2	$V(^{12}C^{16}O)(^{13}C^{16}O)$ (Σ^+)
1674	1671.4	1661	1661.0	$V(^{13}C^{16}O)_2$ (Σ_u^+)
k_{CO} = 12.38		k_{CO} = 12.36		
k_{COCO} = 0.58		k_{COCO} = 0.70		

[a] These modes were too weak to observe under the conditions of our mixed isotope study. [b] See text for details of structural assignments. [c] Infrared inactive.

If one considers the orbitals involved in the bonding scheme of a linear dicarbonyl, then one would qualitatively expect the effectiveness of the metal π overlap from the d_{xz}, d_{yz} set to the π^* orbitals of the CO ligands to diminish as the ∠VCO angle bends toward 90°. The effect of bending the $V(CO)_2$ molecule would therefore be to increase the frequency of the asymmetric CO stretching mode relative to that of the linear form. A rationale of this type would support the assignment of the high-frequency form IIA to the cis-bent dicarbonyl, the intermediate-frequency form IIB to the trans-bent dicarbonyl, and the low-frequency form IIC to the linear dicarbonyl. Molecular orbital calculations described later support this proposal.

Vanadium Monocarbonyl, VCO. The ν(CO) infrared absorption of VCO occurs at 1904, 1890, and 1868 cm^{-1} in Ar, Kr, and Xe matrices, respectively. The red shifts on passing from Ar to Xe are a feature common to all of the $V(CO)_n$ complexes and have been discussed in detail for $Co(CO)_n$.[20] Probably the most interesting property of VCO is the fact that its ν(CO) stretching frequency is surprisingly out of line when compared with FeCO, CoCO, NiCO, and CuCO (1898, 1954, 1996, and 2010 cm^{-1}, respectively).[21] In brief, the series of first-row MCO triatomics has been investigated by extended Hückel molecular orbital techniques[22] assuming a linear geometry. The results of these calculations imply that the CO bond strength on passing from Sc to Cu should increase as seen from the corresponding increase in σ and π CO overlap populations. Charge transfer from the 5σ MO of CO to M increases and from M to the 2π MO of CO decreases on passing from Sc to Cu. Both of these effects result in a strengthening of the CO bond.

On the basis of orbital overlap arguments similar to those outlined earlier for $V(CO)_2$, we are forced to conclude that the anomalously high frequency of VCO can be taken as strong evidence that the predicted Jahn–Teller instability of the molecule has resulted in the formation of a nonlinear monocarbonyl. The following molecular orbital calculations lend credence to both the monocarbonyl and dicarbonyl proposals.

An Extended Hückel Molecular Orbital Investigation of the Effect of Bending ∠VCO and ∠CVC Bonds on the CO Stretching Frequencies of V(CO) and $V(CO)_2$

One method that has been used with some success to determine vibrational frequencies[23] involves the computation of semiempirical molecular orbital wave functions using the iterative extended Hückel method and the use of calculated Mulliken bond overlap populations as a measure of the respective bond stretching force constants (which can then be related to the frequencies). In the case of some simple carbonyls it has been shown that there exists a reasonably good correlation between the CO overlap populations and CO force constants extending over quite a wide range of values (1700 to 2100 cm^{-1}).[23,24]

From our EHMO calculations for linear VCO (utilizing the 3d, 4s, 4p orbitals of V and the 2s, 2p orbitals of C and O), the qualitative energy level scheme which emerges shows that besides the low-lying (bonding) molecular orbitals associated mainly with CO and the V–C σ bond, there exists a group of five orbitals at higher energies which (assuming a low-spin configuration) are composed of a completely filled π set (d_{xz}, d_{yz}), a singly occupied Δ set ($d_{x^2-y^2}$, d_{xy}), and finally an empty Σ^+ (d_{z^2}) orbital. The calculations also indicate very little mixing between the d_{xz}, d_{yz} and $4p_x$, $4p_y$ π orbitals on V, implying that the so-called "back-bonding" from V to the CO ligand is well approximated by the generally accepted $d\pi-\pi^*$ description. Furthermore, in the linear configuration the Δ ($d_{x^2-y^2}$, d_{xy}) set is essentially nonbonding. It would therefore appear that the partitioning of the metal d orbital set into π, Δ, and Σ^+ sets as determined by an EHMO calculation is in effect identical with that which would have been predicted on the basis of a linear crystal field analysis.

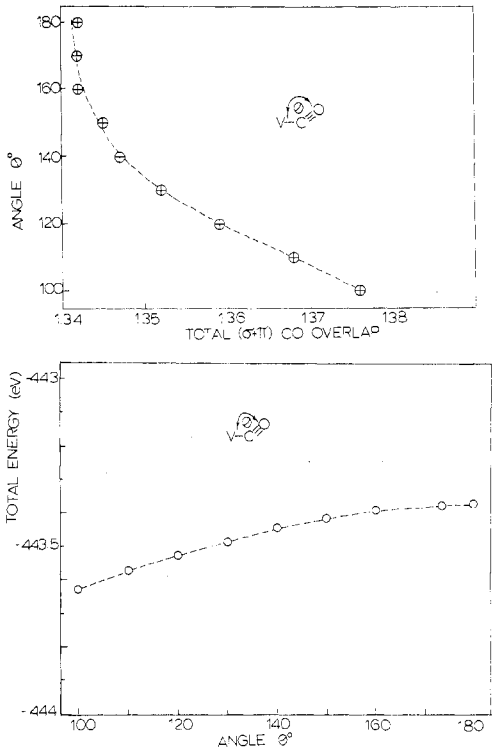

Figure 6. Graphical representation of (A) the total CO orbital overlap population and (B) the internal energy for VCO as a function of the ∠VCO angle in the range 90 to 180°.

By employing the relationship between the Mulliken CO overlap population and the CO bond stretching force constant referred to earlier,[23,24] we find that the CO stretching frequency for VCO is predicted to shift monotonically to higher values as the molecule is distorted from the linear to the nonlinear configuration. Moreover, the total internal energy of VCO decreases as the molecule moves away from the linear geometry. Both of these effects are shown graphically in Figures 6A and 6B for θ = 90 to 180°.

Because the effect of including the 4p orbitals was uncertain, calculations were also performed without the 4p orbitals in the basis set. The only noticeable differences between the two sets of data were (i) a small (~0.5 eV) shift in the overall energy and (ii) a less pronounced yet similar increase in the CO overlap population as the molecule bends from 180 to 90°.

The qualitative conclusion that one can draw from the above calculations is that the anomalously high frequency CO stretching mode observed for VCO (discussed earlier) compared to the other members of the monocarbonyl group (FeCO, CoCO, NiCO, and CuCO) is probably reflecting a nonlinear structure for VCO. This is not unreasonable in view of the predicted Jahn–Teller instability of a low-spin d^5 VCO molecule.

Similar extended Hückel calculations were performed on the three different forms of the dicarbonyl described earlier by varying the ∠VCO angle θ between 90 and 180°.

As with the monocarbonyl, one finds that as the ∠VCO bond angle moves away from 180° toward either a cis C_{2v} or trans C_{2h} configuration, the Mulliken CO overlap population increases and the total internal energy of the molecule decreases. The results of these computations are summarized in Figures 7A and 7B. These results, when taken in conjunction with the $^{12}C^{16}O/^{13}C^{16}O$ isotopic frequency calculations (Table IV) and experimental observations, support the contention that the low-frequency form of the dicarbonyl IIC

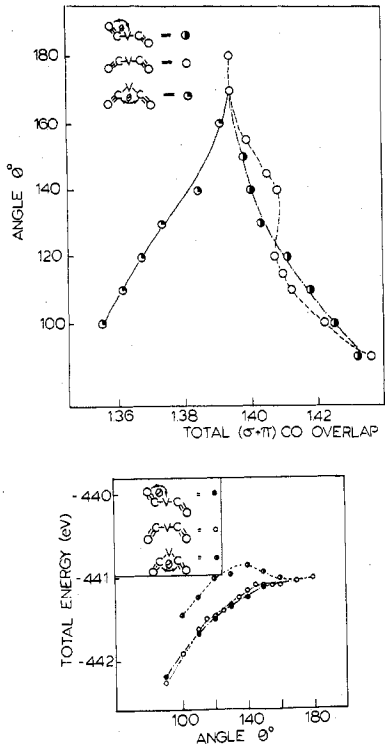

Figure 7. Graphical representation of (A) the total CO orbital overlap population and (B) the internal energy for $V(CO)_2$ as a function of the ∠VCO and ∠CVC angles in the range 90 to 180°.

(k_{CO} = 12.38 mdyn/Å) has the $D_{\infty h}$ linear structure. The Mulliken overlap populations (Figure 7A) suggest that for θ in the range 160–120° the cis C_{2v} dicarbonyl is best assigned to the high-frequency form IIA (k_{CO} = 14.88 mdyn/Å) and the trans C_{2h} dicarbonyl to the intermediate-frequency form IIB (k_{CO} = 13.95 mdyn/Å).

As the difference in energy between the three dicarbonyl configurations for θ in the range 120–180° is of the order or less than 0.5 eV (Figure 2B), it is possible that crystal lattice effects are in part responsible for the isolation of all three complexes at 10–12 K.

Finally, it is interesting to note that extended Hückel calculations show that on bending the dicarbonyl about the vanadium atom, the Mulliken CO overlap population decreases (Figure 7A) rather than increases, in discord with our experimental observations. This behavior, together with the less favorable internal energy for this kind of distortion (Figure 7B), lends credence to our earlier proposal that the high- and intermediate-frequency forms of the dicarbonyls IIA and IIB are best associated with bending of the ∠VCO rather than the ∠CVC bond.

Acknowledgment. We are most grateful to the National Research Council of Canada, the Atkinson Charitable Foundation, Liquid Carbonic, and Erindale College for financial support and to the National Research Council of Canada for a scholarship to L.H.

Registry No. VCO, 59982-45-5; $V^{13}CO$, 59982-46-6; $V(CO)_2$, 59991-85-4; $V(CO)(^{13}CO)$, 59982-47-7; $V(^{13}CO)_2$, 59982-48-8; $V(CO)_3$, 59982-49-9; $V(CO)(^{13}CO)_2$, 59982-50-2; $V(CO)_2(^{13}CO)$, 59982-51-3; $V(^{13}CO)_3$, 59982-52-4; $V(CO)_4$, 59982-53-5; $V(CO)_5$, 59982-54-6.

References and Notes

(1) T. A. Ford, H. Huber, W. Klotzbücher, E. P. Kündig, M. Moskovits, and G. A. Ozin, *Inorg. Chem.*, **15**, 1666 (1976).
(2) T. A. Ford, H. Huber, W. Klotzbucher, E. P. Kündig, M. Moskovits, and G. A. Ozin, *J. Chem. Phys.*, in press.
(3) M. Moskovits and G. A. Ozin, *J. Appl. Spectros.*, **26**, 481 (1972).
(4) E. P. Kündig, M. Moskovits, and G. A. Ozin, *J. Mol. Struct.*, **14**, 137 (1972).
(5) L. Hanlan and G. A. Ozin, *J. Am. Chem. Soc.*, **96**, 6324 (1974).
(6) R. Hoffmann, *J. Chem. Phys.*, **39**, 1397 (1963); R. Hoffmann and W. N. Lipscomb, *ibid.*, **36**, 2179, 3489 (1962); **37**, 2872 (1962).
(7) E. Clementi and D. C. Raimondi, *J. Chem. Phys.*, **38**, 2086 (1963).
(8) J. W. Richardson, R. R. Powell, and W. C. Nieuwpoort, *J. Chem. Phys.*, **38**, 796 (1963).
(9) L. C. Cusachs, *J. Chem. Phys.*, **43**, 5157 (1965).
(10) H. Basch, A. Viste, and H. B. Gray, *J. Chem. Phys.*, **41**, 10 (1968); and *Theor. Chim. Acta*, **3**, 458 (1965).
(11) E. P. Kündig, M. Moskovits, and G. A. Ozin, *Angew. Chem., Int. Ed. Engl.*, **14**, 292 (1975).
(12) G. Blyholder and M. C. Allen, *J. Am. Chem. Soc.*, **91**, 3158 (1969).
(13) J. K. Burdett, *J. Chem. Soc., Faraday Trans. 2*, **70**, 1599 (1974).
(14) M. Elian and R. Hoffmann, *Inorg. Chem.*, **14**, 375 (1975).
(15) J. K. Burdett, *Inorg. Chem.*, **14**, 375 (1975).
(16) R. S. Nyholm and R. J. Gillespie, *Q. Rev., Chem. Soc.*, **11**, 339 (1957); R. J. Gillespie, *J. Chem. Educ.*, **40**, 295 (1963).
(17) M. A. Graham, Ph.D. Thesis, University of Cambridge, 1971.
(18) D. G. Schmidling, *J. Mol. Struct.*, **24**, 1 (1975).
(19) F. A. Cotton and C. S. Kraihanzel, *J. Am. Chem. Soc.*, **84**, 4432 (1962).
(20) L. Hanlan, H. Huber, E. P. Kündig, B. McGarvey, and G. A. Ozin, *J. Am. Chem. Soc.*, **97**, 7054 (1975).
(21) M. Moskovits and G. A. Ozin, "Vibrational Spectra and Structure", J. Durig, Ed., Elsevier, Amsterdam, 1975.
(22) E. P. Kündig and G. A. Ozin, unpublished results.
(23) E. L. Wagner, *J. Chem. Phys.*, **43**, 2728 (1965); K. G. Caulton and R. F. Fenske, *Inorg. Chem.*, **7**, 1273 (1968); A F. Schreiner and T. L. Brown, *J. Am. Chem. Soc.*, **90**, 3366 (1968); J. Alster and M. J. Gallagher, *Mol. Phys.*, **25**, 649 (1973).
(24) P. Politzer and S. D. Kasten, *Surf. Sci.*, **36**, 186 (1973); and *J Phys. Chem.*, **80**, 283 (1976).
(25) Weak shoulders at approximately 1896 and 1712 cm^{-1} were shown from isotope substitution experiments to arise from multiple trapping site effects.